RESEARCH ARTICLE
doi: 10.2306/scienceasia1513-1874.2026.s002
ScienceAsia 52S (1): 2026: ID 2026s002: **1–8**

The one-dimensional model of state transition in magnetized plasma based on bifurcation analysis

Thiti Aungcharoen[a], Danis Klanurak[a], Nopporn Poolyarat[b], Jiraporn Promping[b], Arlee Tamman[b], Apiwat Wisitsorasak[c], Ponkris Klaywittaphat[d], Boonyarit Chatthong[a,*]

[a] Division of Physical Science, Faculty of Science, Prince of Songkla University, Songkhla 90110 Thailand
[b] Thailand Institute of Nuclear Technology, Nakhon Nayok 26129 Thailand
[c] Department of Physics, Faculty of Science, King Mongkut's University of Technology Thonburi, Bangkok 10140 Thailand
[d] Faculty of Engineering, Thaksin University, Phatthalung 93210 Thailand

*Corresponding author, e-mail: boonyarit.ch@psu.ac.th

Received 29 Dec 2025, Accepted 24 Aug 2026
Available online

ABSTRACT: The occurrence of limit-cycle oscillations during the low to high confinement mode transition in magnetically confined plasma is investigated using bifurcation theory. The fixed-point and stability analyses of the minimal temporal model are carried out, revealing two distinct critical external power thresholds. The first corresponds to the onset of limit-cycle oscillation via Hopf bifurcation in which plasma turbulence and zonal flow shear form a self-regulating state. The second is associated with the transcritical bifurcation that drives the system into high confinement mode where mean flow shear sustains turbulence suppression. The minimal temporal model is extended to a spatio-temporal model by coupling it to the energy transport equation and allowing for the turbulence spreading effect. In this model, the limit-cycle orbit originates at the plasma edge due to pressure gradient driven linear instability. During each cycle, the turbulence and zonal flow fronts also propagate radially inward due to turbulence spreading effect. Once the external power threshold surpasses the second critical value, an edge transport barrier is formed self-consistently at the edge of plasma pressure profile, providing rapidly strong mean flow shear that sustains local turbulence suppression and prevents the back-transition to the low confinement mode.

KEYWORDS: fusion plasma, transition dynamics, limit-cycle oscillations, turbulence-flow shear interaction

MSC2020: 76X05 37G15 76F25 35Q35

INTRODUCTION

Magnetic confinement fusion aims to achieve sustained thermonuclear reactions by maintaining a high-temperature plasma within strong magnetic fields. Among the various operational regimes, the high-confinement mode (H-mode) plays a crucial role because it significantly improves plasma energy confinement compared with the low-confinement mode (L-mode) [1]. For next-step fusion devices, such as the International Thermonuclear Experimental Reactor (ITER) and DEMOnstration power plant (DEMO), accessing and maintaining H-mode is crucial for achieving the plasma conditions necessary for efficient fusion power production. Despite its importance, the transition from L-mode to H-mode, commonly referred to as the L-H transition, remains one of the most complex nonlinear phenomena in plasma physics, involving multiscale interactions among plasma turbulence, zonal flow shear, and mean flow shear [2].

A key feature observed in the vicinity of the L-H transition is the emergence of limit-cycle oscillations (LCOs)—quasi-periodic oscillations in edge turbulence and flow shear [3–6]. These oscillations arise from the dynamic competition between turbulence drive and shear suppression, providing detailed information on the self-regulation processes governing confinement transitions. Predicting the LCO phase is important because it provides an early indicator that the plasma is approaching the L-H transition. Since LCOs arise from the self-regulating interaction between turbulence and shear flows, their onset, amplitude, and duration contain useful information about the heating power threshold and the nonlinear mechanisms that lead to H-mode access. A reliable prediction of the LCO phase can therefore help clarify the physical route from L-mode to H-mode and may provide guidance for optimizing external heating scenarios and confinement control in future fusion devices. The multi-predator–one-prey model is a widely used theoretical framework for describing LCO behavior [7]. In this model, turbulence acts as the prey, while zonal-flow (ZF) shear and mean-flow (MF) shear serve as competing predators that suppress turbulence growth through shear-induced turbulence decorrelation. The corresponding energy causality is illustrated in Fig. 1. Turbulence extracts free energy from the pressure gradient through linear instabilities and transfers its energy to zonal flows via Reynolds stress. The generated zonal flows subsequently suppress turbulence, reducing turbulent transport and allowing the pressure gradient to recover. On a slower time scale, mean-

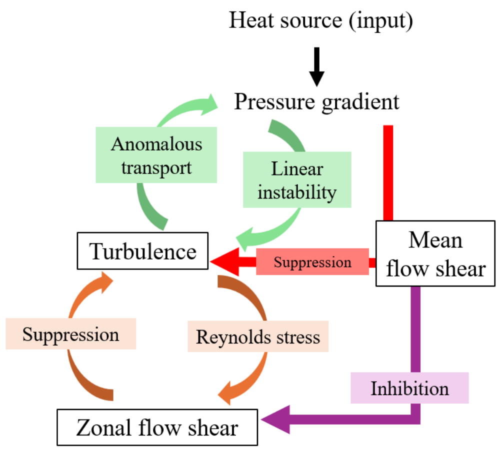

Fig. 1 The energy causality among plasma turbulence, zonal-flow shear, and mean-flow shear

flow shear also suppresses turbulence and inhibits the growth of zonal flows. The interplay among these mechanisms forms a self-regulating feedback loop that gives rise to LCO behavior. Earlier studies have shown that this minimal temporal model captures essential features of the L-H transition and describes the existence of multiple equilibrium states, also known as fixed points, bifurcation structures, and the occurrence of LCOs [8, 9] under a certain set of model parameters. However, temporal models alone are insufficient to describe the formation of the edge transport barrier (ETB), which characterizes H-mode. This is because the ETB formation is intrinsically spatial and arises from the coupled effects of pressure-gradient drive, turbulence spreading [10, 11], and localized shear-flow generation near the plasma edge. To address this limitation, the temporal predator-prey model must be extended to a spatio-temporal system by coupling it with the one-dimensional energy transport equation [12] and allowing for turbulence spreading effect.

In this work, we investigate the dynamical behavior of the L-H transition using both temporal and spatio-temporal formulations of the predator-prey models. We perform fixed-point and stability analyses to identify the multiple equilibrium states of the system and to track how their stability changes as the controlled parameter is varied. Two distinct critical power thresholds emerge from the bifurcation analysis: (1) a first threshold associated with a Hopf bifurcation, marking the onset of limit-cycle oscillations, and (2) a second threshold corresponding to a transcritical bifurcation, after which the turbulence-free state becomes only stable state.

Although spatio-temporal models have previously been proposed to describe the L-H transition with the preceding LCO-phase [13, 14], these formulations typically rely on a slow, linear power ramp-up, during which the models can reproduce the emergence of the LCO phase. However, under such conditions it becomes difficult to determine the precise location of the limit-cycle orbit, as its size continuously evolves with the increasing heat source. Consequently, the system trajectory may not actually converge onto a stable limit cycle; instead, it spirals inward and outward throughout the transition driven by the linear power ramp-up. Moreover, a strictly linear power-ramp scenario is not always experimentally achievable. In this work, we address these limitations by employing a simplified version of the spatio-temporal model with a step-like external heat source. In this study, the external heat source is prescribed in a step-like form to mimic an abrupt increase in externally injected heating power, such as neutral beam injection, electron or ion cyclotron microwave heating. The step-like profile is not intended to represent a specific actuator waveform, but rather an idealized heating scenario that allows the nonlinear system to relax to each dynamical state before the next power level is applied. This makes it possible to identify the limit-cycle orbit more clearly than in a continuously ramped heating case. This approach enables a clear identification of the limit-cycle orbit in the three-dimensional phase space, as the abrupt heating allows the system trajectory to fully settle onto the limit cycle before subsequently transitioning to the H-mode regime.

By incorporating turbulence spreading and pressure-gradient-driven instabilities, the spatio-temporal extension reproduces key observations, including the edge localized onset of LCOs and the inward propagation of turbulence and zonal-flow fronts. Above the second power threshold, the model predicts the spontaneous formation of a robust edge transport barrier that sustains strong mean-flow shear and suppresses turbulence, thereby preventing back-transition to L-mode. In summary, this study provides a unified theoretical description of confinement transitions in magnetically confined plasma, highlighting the central roles of bifurcations, multi-predator–prey interactions, and radial transport processes. The results contribute to a deeper understanding of the physics underlying H-mode access and hold implications for optimizing plasma performance in future fusion reactors.

SPATIO-TEMPORAL MULTI-PREDATOR–ONE-PREY MODEL

It is believed that the occurrence of LCOs in magnetic confinement devices arises from the nonlinear and complex interactions among plasma turbulence, ZF shear, and MF shear. These dynamics can be described using the minimal temporal multi-predator–one-prey model [7, 8, 15], in which the ZF and MF shears act as competing predators that suppress the plasma turbulence, which in turn behaves as the prey. A detailed description of the temporal model is provided in [7]. To self-consistently describe the formation of an edge transport barrier (ETB), which develops at the plasma edge, the temporal model must be extended to include spatial effects. This can be achieved by coupling the temporal model with the one-dimensional energy transport equation and allowing for turbulence spreading effect. The resulting extended model captures the space-time evolution of turbulence intensity (I), zonal flow shear energy ($E_{\mathrm{ZF}} = V_{\mathrm{ZF}}'^2$), and plasma pressure ($p$). The model can be written as follows:

$$\frac{\partial I}{\partial t} = \left[\gamma_L I - \alpha_{\mathrm{ZF}} E_{\mathrm{ZF}} I - \alpha_{\mathrm{MF}} E_{\mathrm{MF}} I - \Delta\omega I^2\right] \tag{1}$$

$$+ \chi_N \frac{\partial}{\partial y} I \frac{\partial I}{\partial y}, \tag{2}$$

$$\frac{\partial E_{\mathrm{ZF}}}{\partial t} = \frac{\alpha_{\mathrm{ZF}} I}{1 + \zeta_0 E_{\mathrm{MF}}} E_{\mathrm{ZF}} - \gamma_d E_{\mathrm{ZF}}, \tag{3}$$

$$\frac{\partial p}{\partial t} = \frac{\partial}{\partial y}\left[(\chi_{\mathrm{neo}} + \chi_{\mathrm{turb}}) \frac{\partial p}{\partial y}\right] + Q_0\, \mathrm{e}^{\left(\frac{-y^2}{2L_{\mathrm{p,dep}}^2}\right)}. \tag{4}$$

Predator-prey system

Equations (1) and (3) exhibit the characteristics of a predator-prey system, where turbulence intensity (prey) emerges first and subsequently transfers part of its energy to the zonal flow (the first predator) via three-wave nonlinear interaction. The zonal flow, in turn, interacts back with the turbulence through a suppression mechanism, resulting in a self-regulating dynamics [2]. The first term on the right-hand side (RHS) of Eq. (1) represents the growth of turbulence driven by a linear instability, with the turbulence growth rate γ_L defined as:

$$\gamma_L = \alpha_I \left(\frac{c_s}{R}\right) \sqrt{\left\{\frac{R}{L_p} - \left(\frac{R}{L_p}\right)_{\mathrm{cri}}\right\} \Theta \left\{\frac{R}{L_p} - \left(\frac{R}{L_p}\right)_{\mathrm{cri}}\right\}}, \tag{5}$$

where α_I denotes the strength of the growth rate, R is the plasma major radius, and $L_p^{-1} = |\mathrm{d}\ln p/\mathrm{d}y|$ is the inverse pressure gradient scale length. The term $(R/L_p)_{\mathrm{cri}}$ corresponds to the critical threshold of plasma pressure gradient, and Θ is the Heaviside function. The second and third terms describe the suppression of turbulence by ZF and MF shears with coupling coefficients α_{ZF} and α_{MF}, respectively. The fourth term accounts for the nonlinear saturation of turbulence. These terms enclosed within the square brackets represent the locality effect of the turbulence intensity, while the final term introduces the non-local turbulence self-scattering, which originates from nonlinear mode-coupling in wavenumber space [16], with turbulent thermal diffusivity χ_N. When the pressure gradient exceeds its critical value, the turbulence is excited and propagates toward the region of weaker excitation. Consequently, turbulence can penetrate into linearly stable region of the plasma [17], leading to the enhancement of turbulent energy cross-field transport and degradation of the energy confinement.

The first term on the RHS of Eq. (3) represents the excitation of the zonal flow as turbulence is sufficiently strong to overcome the linear flow damping γ_d (the second term). The MF shear also inhibits the growth of zonal flow with the inhibition strength ζ_0. It is worth noting that the evolution of zonal flow shear energy does not explicitly depend on the spatial effect by itself, on the other hand, it depends on the space-time evolution of the turbulence intensity and mean flow shear through excitation and inhibition effects, respectively.

One-dimensional energy transport equation

The mean flow shear energy $E_{\mathrm{MF}} = V_{E\times B}'^2$, the second predator, can be obtained by the radial force balance equation: $V_{E\times B}' \approx \rho_s c_s / L_p^2$, where we only consider the diamagnetic shear under the assumption of frozen density profile to simplify the analysis and prevent numerical instabilities. Moreover, we also neglect the contribution of pressure profile curvature, and poloidal and toroidal magnetic fields. The space-time evolution of plasma pressure in the mean flow shear calculation can be obtained by the one-dimensional energy transport equation. The terms enclosed within square brackets of Eq. (4) is the diffusive energy flux comprises the neoclassical and turbulent thermal diffusivities. The former is given by:

$$\chi_{\mathrm{neo}} = \left(\frac{R}{a}\right)^{3/2} q^2 \rho_s^2 \nu_{ii}, \tag{6}$$

which is the collisional thermal diffusivity in the Banana regime. The parameter $q = 1 + 2(y/a)^2$ is the simplified formal magnetic q-profile and ν_{ii} is the ion-ion collision frequency. The latter is given by

$$\chi_{\mathrm{turb}} = \frac{a c_s I}{1 + \alpha_t E_{\mathrm{MF}}}, \tag{7}$$

where it is self-consistently coupled to the turbulence intensity evolution rather than assumed to be constant as done in the previous works [18, 19]. Here, α_t is the cross-phase modification of turbulent transport by the mean flow shear, providing the strength of the turbulent transport suppression. The last term on the RHS of Eq. (4) represents the flux-driven external heat source providing the free energy into the system, where Q_0 is the amplitude of the Gaussian heat source localized at the plasma core and $L_{\mathrm{p,dep}}$ is the energy deposition width.

Fixed-point and stability analyses

Under certain limits, the spatio-temporal model can be reduced to the temporal model. Thus, the multiple equilibrium states and their dynamics are equivalent.

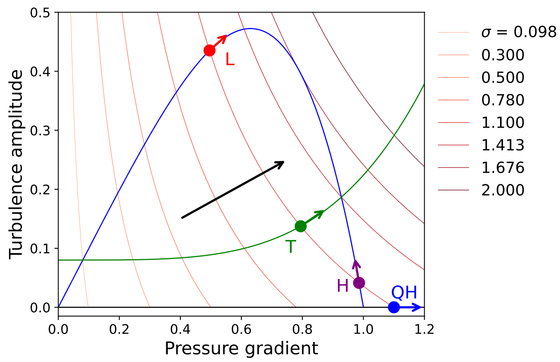

Fig. 2 The equivalent phase portrait of the temporal model projected onto the plane without zonal flow for different heat source σ. The black arrow indicated the direction of increasing in heat source. The shown fixed points are calculated at $\sigma = 1.1$.

In this section, we carry out the fixed-point and stability analyses of the temporal model in which the results can be qualitatively adapted to describe the dynamics of spatio-temporal model. The analysis procedures are similar to those in [8, 9]. The general procedures can be explained as follows: first, by considering the system at steady state, we obtain the nullclines of the system, where their intersections represent the location of fixed points in the phase space. Second, to determine the type and stability of each fixed point, we perform linearization by evaluating the Jacobian matrix of the system of equations at each corresponding fixed point and look for the eigenvalues, which contain the information of each equilibrium state [20]. Once the controlled parameter is varied, the dynamic of each fixed point will change as the eigenvalues also change. In this work, the external heat source is chosen as a control parameter to mimic the heating scenario in the actual fusion experiment.

The phase portrait between plasma turbulence and pressure gradient projected onto the plane without zonal flow shear carried out by the fixed-point analysis of the temporal model is shown in Fig. 2. The colored curves and black horizontal line represent the nullclines of the system. The darker red curves correspond to the nullclines with higher external heat source, while other nullclines are fixed as the heat source is varied. The red, green, purple, and blue dots represent the locations of the L-, T-, H-, and QH-mode fixed point, respectively. Note that the name of each fixed point is preserved to be the same as those in [8]. The time evolution of these fixed points under varying heat sources is illustrated by arrows, each matching the color of the respective mode, i.e., each fixed point move along the nullclines as the controlled parameter is varied. Here, σ denotes the normalized external heating strength used as the control parameter in the reduced temporal bifurcation analysis. Increasing σ corresponds to increasing the externally applied heating power. The value $\sigma = 1.1$ is selected as a representative case because it lies in the intermediate regime where the L-, T-, H-, and QH-mode fixed points can be clearly displayed and compared.

The stability analysis of the temporal model reveals that there are two distinct critical values in the external heat source. Surpassing the first one causes the T-mode fixed point loses its stability and undergoes Hopf-bifurcation giving rise to the LCO behavior. On other hands, surpassing the second one gives rise to the transcritical bifurcation where the LCO is terminated and the system transits to the state without turbulence and zonal flow as this state is the only possible stable state. In the next section, we will use this information to look for the occurrence of the LCO during the L-H transition in the spatio-temporal model.

Table 1 Model parameters used in the simulations.

Parameter	Value	Parameter	Value
ρ_s	10^{-2}	$\Delta\omega$	2.5×10^{-3}
R	4	α_{ZF}	10
a	1	α_{MF}	4.5×10^{-3}
α_t	0.1	ζ_0	10^2
χ_N	5.0×10^{-3}	γ_d	7.5×10^{-4}
α_I	2.5×10^{-3}	$L_{\mathrm{p,dep}}$	0.12
$(R/L_p)_{\mathrm{cri}}$	3.7	ν_{ii}	3.0×10^{-3}

Numerical simulation setup

The system of partial differential equations (1) to (4) are numerically solved by BOUT++ fluid simulation framework [21]. We impose fixed boundary condition for the edge pressure, i.e., $p = 0.01$, while other boundaries are set to Neumann conditions. The model parameters are shown in Table 1, which are similar to those used in the literature. However, since our model is the simplified version, some parameters need to be adjusted to satisfy the Hopf bifurcation criterion and to avoid numerical instability especially during the LCO-phase where the pressure gradient changes drastically. We utilize the CVODE time integrator for time evolution. The finite volume method is employed to discretize the diffusion terms. The pressure gradient is calculated via the fourth-order central finite difference method. The radial coordinate y and time t are normalized by the minor radius a and drift-wave time scale a/c_s, respectively. Here $c_s = \sqrt{T_{i0}/m_i}$ is the ion sound speed with reference ion temperature $T_{i0} = 1$ keV and m_i is the ion mass. A uniform grid spacing of 1/256 and time step of 10 are used. The numerical simulations are performed with LANTA supercomputer in Thailand.

RESULTS AND DISCUSSIONS

LCO during L-H transition

This section investigates the occurrence of the LCO during the L-H transition with the spatio-temporal

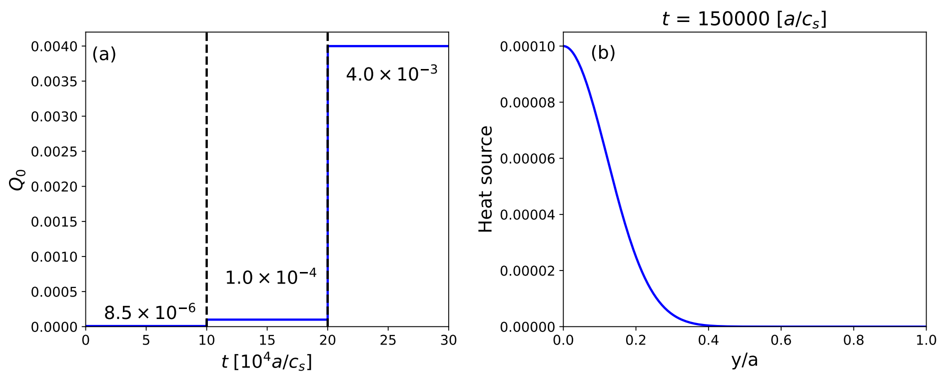

Fig. 3 (a) Time history of the amplitude of the Gaussian heat source. (b) Radial profile of the Gaussian heat source at $t = 150000\ a/c_s$.

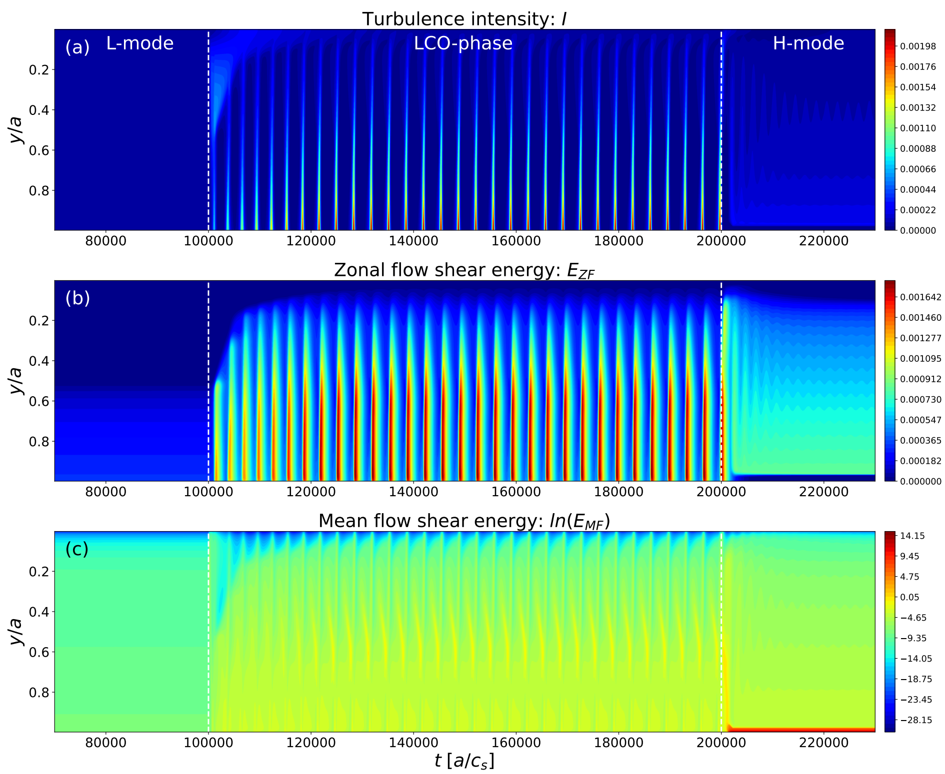

Fig. 4 Space-time evolution of (a) turbulence intensity, (b) ZF shear energy, and (c) MF shear energy during a step change in the external heat source. Limit-cycle oscillations emerge in the intermediate regime between L-mode and H-mode. In the H-mode, the MF shear becomes dominant within the edge transport barrier (ETB) region.

model under a step external heat source. The time history and typical radial profile of the heat source are shown in Fig. 3 (a) and (b), respectively.

During the first phase of the heating scenario, the amplitude of the Gaussian source is below the first critical point. As a result, an arbitrary initial condition evolves and saturates at the stable spiral fixed point where turbulence and zonal flow remain at low levels characterized as the L-mode state. The space-time evolution of turbulence intensity, ZF shear energy, and MF shear energy during the L-mode is shown as the first phase of Fig. 4 (a) to (c), respectively. Once the amplitude of the Gaussian source surpass the first critical point, the stable spiral fixed point loses its stability, resulting in the Hopf bifurcation hence the LCO behavior as shown in the second phase of Fig. 4. Notice that, the amplitude of the each model species keep growing at the beginning of the LCO-phase then oscillate with a finite amplitude. This is because as soon as the heat source exceeds the first critical point, the unstable spiral fixed point pushes the trajectories away from it then they are attracted and settled down to the limit cycle orbit. Once the heat source surpass the second critical point, the LCO behavior terminates

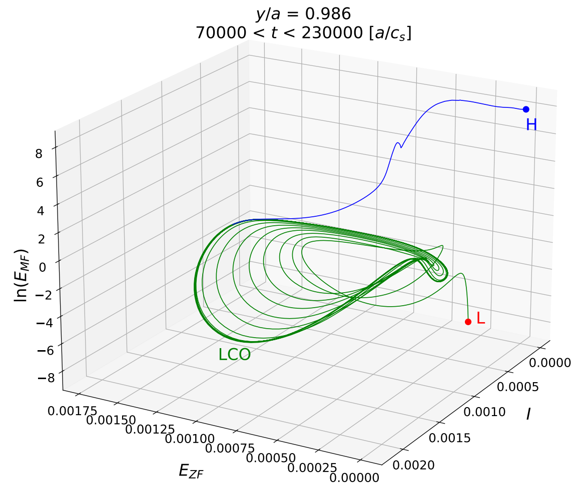

Fig. 5 Three dimensional phase space showing L-LCO-H transition. The limit cycle orbit is shown as the circumference of the cycle in green.

then the trajectories are attracted to the new fixed point characterized as the H-mode state. In the H-mode, the rapid steep pressure gradient forms a very strong mean flow shear, which then suppresses turbulence intensity and anomalous transport. This results in the formation of the ETB in the pressure profile. In addition, since zonal flows are driven by turbulence, without the driving term zonal flow also disappears in the ETB region during the H-mode.

The three-dimensional phase space among edge turbulence intensity, ZF shear energy, and MF shear energy during L-LCO-H transition via a step heating scenario is illustrated in Fig. 5. Note that the trajectory during L-mode regime start at $t = 70000\ a/c_s$ where the system already reached the first equilibrium state. The initial oscillations as initial condition spiral toward equilibrium point are not shown here. The steady limit cycle orbit is shown at the circumference of the cycle in green.

Steady-state radial profiles

The radial profiles of turbulence intensity, ZF shear energy, MF shear energy, and plasma pressure during each state are shown in Fig. 6 (a) to (d), respectively. Note that the time slice of the LCO-phase in green is selected at the specific time of maximum level of the turbulence intensity during a certain steady limit cycle. It can be seen that turbulence and zonal flow co-exist in the edge region during the L-mode then they propagate radially inward due to the turbulence spreading effect during the LCO-phase. In addition, they dominate over most of the plasma area except for the deep core region. Interestingly, the turbulence intensity at a certain limit cycle is very strong in this phase. This may explain the bursty dynamics of turbulence amplitude measured by several diagnostics

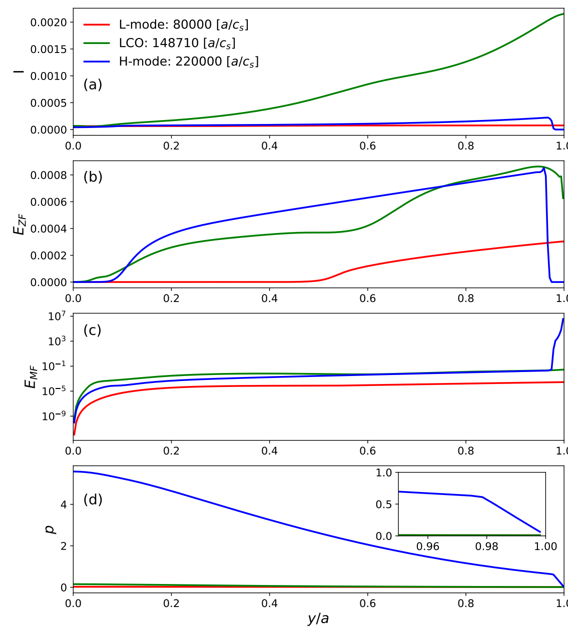

Fig. 6 Radial profiles of (a) turbulence intensity, (b) ZF shear energy, (c) MF shear energy, and (d) plasma pressure during the L-mode (red), LCO phase (green), and H-mode (blue). The inset in the pressure profile highlights the formation of the ETB at the plasma edge.

[22–24]. The ETB formation during the H-mode is clearly formed self-consistently in the edge region of the plasma pressure as shown in the inset of Fig. 6 (d). In this region the MF shear is very strong that capable to suppress the anomalous transport that later prevent the regeneration of the turbulence intensity in this region. In other words, the MF shear is responsible for the sustainment of the turbulence suppression in the H-mode rather than forming a self-regulation loop as done by the ZF shear during LCO-phase.

Predator-prey relationship during LCO-phase

In order to confirm the predator-prey relationship between turbulence (prey) and zonal flow (predator) as the former appears first then transfers its energy to the latter via the Reynolds stress, the time evolution of both quantities is shown in Fig. 7 (a). It is obvious that the turbulence peaks lead the zonal flow peaks consistent with the predator-prey type relationship. This can also be confirmed by the cross-correlation function between ZF shear energy and turbulence intensity $C(E_{\mathrm{ZF}}, I)$ where the maximum correlation function appears at the positive time lag, indicating the zonal flow shear energy lag the turbulence intensity.

CONCLUSION

In this work, we employed a simplified spatio-temporal multi-predator–one-prey model to demonstrate the emergence of limit-cycle oscillations during the L-H transition under a step-like external heat source. Un-

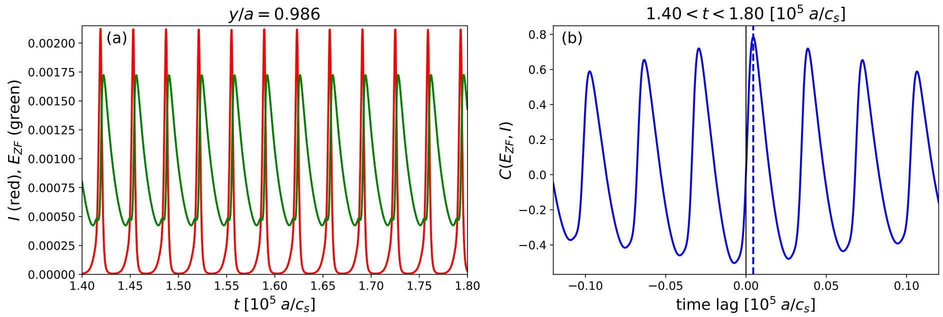

Fig. 7 (a) Time evolution of the edge turbulence intensity and ZF shear energy during the steady LCO phase. (b) Cross-correlation function between the ZF shear energy and turbulence intensity, evaluated over the same time interval as in (a), showing a peak at positive time lag, which indicates that the ZF shear response lags the turbulence drive.

like the case of a linear power ramp-up, in which the system trajectories spiral inward and outward without fully converging, the step-heating scenario allows the trajectories to settle onto a well-defined limit-cycle orbit. This enables a precise identification of the limit cycle orbit in the three-dimensional phase space. The model further shows that the edge transport barrier forms self-consistently at the plasma edge, coinciding with regions of strong mean flow shear that sustain turbulence suppression. Future work will focus on extending the model by incorporating the particle transport equation to achieve a more comprehensive description of edge dynamics.

Acknowledgements: This work is partially supported by Thailand Science Research and Innovation (TSRI) Fundamental Fund project number 204519. The authors gratefully acknowledge The National Science and Technology Development Agency (NSTDA) Supercomputer Center (ThaiSC), Pathum Thani, Thailand, for providing computing resources for this study. T. Aungcharoen thanks to the Development and Promotion of Science and Technology Talents Project (DPST) scholarship for financial support. B. Chatthong acknowledges TINT to University Program.

REFERENCES

1. Wagner F, Becker G, Behringer K, Campbell D, Eberhagen A, Engelhardt W, Fussmann G, Gehre O, et al (1982) Regime of improved confinement and high beta in neutral-beam-heated divertor discharges of the asdex tokamak. *Phys Rev Lett* **49**, 1408–1412.
2. Diamond PH, Itoh SI, Itoh K, Hahm TS (2005) Zonal flows in plasma: A review. *Plasma Phys Controlled Fusion* **47**, R35.
3. Estrada T, Happel T, Hidalgo C, Ascasíbar E, Blanco E (2010) Experimental observation of coupling between turbulence and sheared flows during L-H transitions in a toroidal plasma. *Europhys Lett* **92**, 35001.
4. Schmitz L, Zeng L, Rhodes TL, Hillesheim JC, Doyle EJ, Groebner RJ, Peebles WA, Burrell KH, et al (2012) Role of zonal flow predator-prey oscillations in triggering the transition to H-Mode confinement. *Phys Rev Lett* **108**, 155002.
5. Xu G, Wang H, Xu M, Wan B, Guo H, Diamond P, Tynan G, Chen R, et al (2014) Dynamics of L-H transition and I-phase in east. *Nucl Fusion* **54**, 103002.
6. Howlett L, Cziegler I, Freethy S, Meyer H, the MAST team (2023) L-H transition studies on mast: power threshold and heat flux analysis. *Nucl Fusion* **63**, 052001.
7. Kim Ej, Diamond PH (2003) Zonal flows and transient dynamics of the $L-H$ transition. *Phys Rev Lett* **90**, 185006.
8. Malkov MA, Diamond PH (2009) Weak hysteresis in a simplified model of the L-H transition. *Phys Plasmas* **16**, 012504.
9. Dam M, Brøns M, Juul Rasmussen J, Naulin V, Xu G (2013) Bifurcation analysis and dimension reduction of a predator-prey model for the L-H transition. *Phys Plasmas* **20**, 102302.
10. Gürcan ÖD, Diamond PH, Hahm TS, Lin Z (2005) Dynamics of turbulence spreading in magnetically confined plasmas. *Phys Plasmas* **12**, 032303.
11. Singh R, Diamond PH (2020) When does turbulence spreading matter? *Phys Plasmas* **27**, 042308.
12. Hinton FL (1991) Thermal confinement bifurcation and the L- to H-mode transition in tokamaks. *Physics of Fluids B Plasma Physics* **3**, 696–704.
13. Miki K, Diamond PH, Gürcan ÖD, Tynan GR, Estrada T, Schmitz L, Xu GS (2012) Spatio-temporal evolution of the L → I → H transition. *Phys Plasmas* **19**, 092306.
14. Li X, Guo Z, Diamond PH (2024) Formation, propagation and conversion of transport barriers triggered by dynamical critical gradient in tokamak plasmas. *Nucl Fusion* **64**, 044001.
15. Li X, Guo Z, Zhao K (2020) A model of heat pulse induced limit-cycle-oscillations in the edge of magnetically confined plasmas. *Plasma Phys Controlled Fusion* **62**, 125018.
16. Heinonen RA, Diamond PH (2020) A closer look at turbulence spreading: How bistability admits intermittent, propagating turbulence fronts. *Phys Plasmas* **27**, 032303.
17. Hahm TS, Diamond PH, Lin Z, Itoh K, Itoh SI (2004) Turbulence spreading into the linearly stable zone and transport scaling. *Plasma Phys Controlled Fusion* **46**, A323.
18. Chatthong B, Onjun T (2015) Understanding roles of $E\times B$ flow and magnetic shear on the formation of internal and edge transport barriers using two-field bifurcation

concept. *Nucl Fusion* **56**, 016010.

19. Klanurak D, Dang-iad A, Promping J, Poolyarat N, Sangaroon S, Wisitsorasak A, Klaywittaphat P, Chatthong B (2024) Effects of neoclassical and anomalous transport on elm dynamics based on three-field bifurcation model. *ScienceAsia* **50**, 2024s004.
20. Strogatz SH (2015) *Nonlinear Dynamics and Chaos: With Applications to Physics, Biology, Chemistry, and Engineering*, 2nd edn, CRC Press, Boca Raton, FL.
21. Dudson B, Umansky M, Xu X, Snyder P, Wilson H (2009) BOUT++: A framework for parallel plasma fluid simulations. *Comput Phys Commun* **180**, 467–1480.
22. Tynan G, Xu M, Diamond P, Boedo J, Cziegler I, Fedorczak N, Manz P, Miki K, et al (2013) Turbulent-driven low-frequency sheared $E \times B$ flows as the trigger for the h-mode transition. *Nucl Fusion* **53**, 073053.
23. Cheng J, Dong JQ, Itoh K, Yan LW, Xu M, Zhao KJ, Hong WY, Huang ZH, et al (2013) Dynamics of low-intermediate–high-confinement transitions in toroidal plasmas. *Phys Rev Lett* **110**, 265002.
24. Jones C, Andrew Y, Ashton-Key T, Federici F, Kim E, Rhodes T, Scannell R (2025) Spatio-temporal turbulence dynamics over the MAST-U edge transport barrier evolution. *Plasma Phys Controlled Fusion* **67**, 082501.